Article

Characterization and Efficacy of a Nanomedical Radiopharmaceutical for Cancer Treatment

Ingrid Yao Mattisson, Sania Bäckström, Erik Ekengard, Sujinna Lekmeechai, Yi-Chi Liu, Juraj Paris, Rodrigo Petoral, Marie Sydoff, Mats Hansen, and Oskar Axelsson*

Read Online

ACCESS | Metrics & More | Article Recommendations | Supporting Information

ABSTRACT: Although much progress has been made over the last decades, there is still a significant clinical need for novel therapies to manage cancer. Typical problems are that solid tumors are frequently inaccessible, aggressive, and metastatic. To contribute to solving some of these issues, we have developed a novel radioisotope-labeled 27 nm nanoparticle, ^{177}Lu-SN201, to selectively target solid tumors via the enhanced permeability and retention effect, allowing irradiation intratumorally. We show that ^{177}Lu-SN201 has robust stealth properties in vitro and anti-tumor efficacy in mouse mammary gland and colon carcinoma models. The possible clinical application is also addressed with single photon emission computed tomography imaging, which confirms uptake in the tumor, with an average activity of 19.4% injected dose per gram (ID/g). The properties of ^{177}Lu-SN201 make it a promising new agent for radionuclide therapy with the potential to target several solid tumor types.
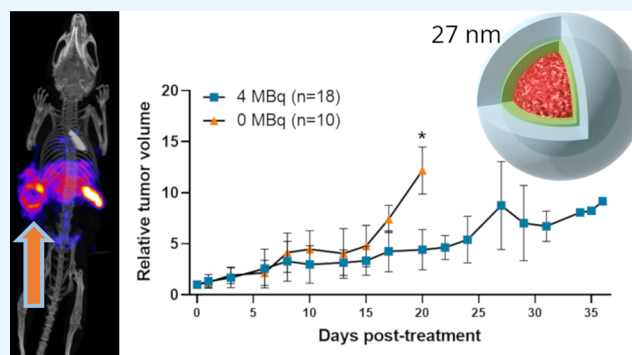
INTRODUCTION

Despite the progress in cancer drug development, patients with late-stage cancer face poor prognoses due to limited treatment options and disease management.[1] Many current treatments fail to provide curative or disease-controlling effects in many settings and are associated with clinical side effects that negatively affect patients' quality of life.[2] In recent years, radionuclide therapy has generated interest due to the internal targeting of tumors with radiation that elicits localized cytotoxic effects.[3] Among the FDA-approved radiotherapies, antibodies and peptides are the leading carriers of radionuclides.[4] Apart from the high production cost of antibodies and peptides, many radioisotope therapies fail to exert the desired anti-tumor effects due to tumor cells' heterogeneity and complex survival mechanisms. Recurrent tumor growth is an effect of a combination of factors: genomic instability, adaptive responses, bystander effect, cellular heterogeneity, and radiation resistance.[5] Consequently, incompletely eradicated tumors allow the selection and expansion of the most resistant tumor cell clones.[6]

A rapidly growing tumor aggressively recruits blood vessels, resulting in immature and leaky capillaries, and at the same time, it lacks efficient drainage of lymphatic systems. These pathophysiological characteristics of solid tumors enable the so-called enhanced permeation and retention (EPR) effect.[7] We have developed a polymeric nanoparticle that selectively accumulates in solid tumors through the EPR effect. The

candidate drug, ^{177}Lu-SN201, delivers locally irradiating ^{177}Lu-radioisotopes into the tumor tissue. In addition, we have demonstrated the tumor accumulating feature with the contrast agent SN132D, another drug candidate developed from the same platform. SN132D recently showed clinically relevant magnetic resonance imaging (MRI) contrast enhancement in breast tumors (EudraCT no. 2018-002193-41).

This study shows that ^{177}Lu-SN201 accumulates in tumor tissue in vivo, with a circulation half-life of 18 to 23 h, with 19.4% ID/g tumor uptake 72 h post-injection, revealed by single photon emission computed tomography (SPECT) imaging. Results show anti-tumor efficacy with a slower tumor growth rate and prolonged survival time significantly in tumor-bearing mouse models of aggressive breast cancer and colon adenocarcinoma. In addition, SPECT imaging shows tumor localization of ^{177}Lu-SN201. The results indicate that ^{177}Lu-SN201 will enable site-specific radiotherapy and non-invasive imaging of advanced solid tumors.

This concept is based on prolongation of the nanoparticle circulation time in blood, to allow time for EPR-driven tumor
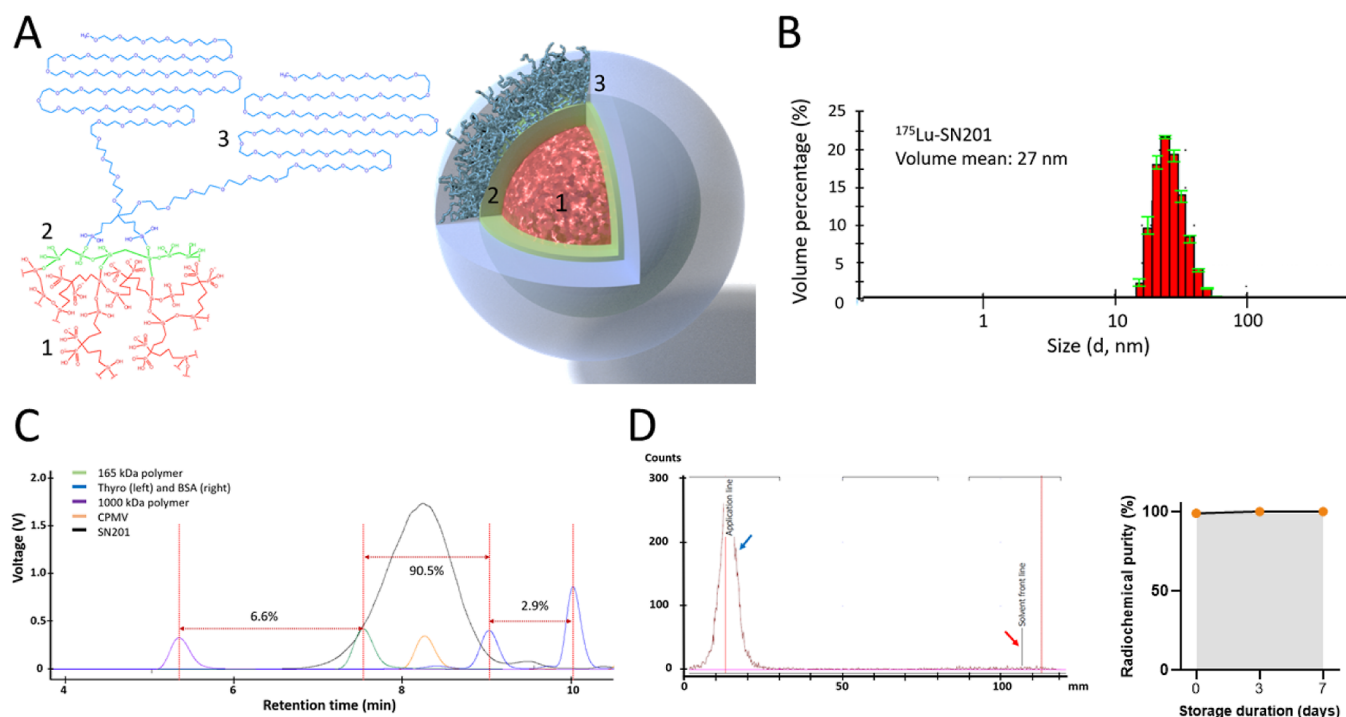
Figure 1. Structure, characterization, and labeling of SN201. (A) SN201 components, (1) BisBis core; (2) anchoring; and (3) PEG coating. (B) Dynamic light scattering (DLS) size characterization of Lu-loaded SN201. Bars present the volume percentage of the diameter ± SD error bars. (C) SEC chromatograms from the evaporative light scattering detector (ELSD) for SN201 (black) and the reference standards: poly(ethylene oxide) (purple), poly(ethylene oxide) (green), CPMV protein (orange), and 1:1 thyroglobulin: BSA mixture (blue). (D) Instant thin layer chromatography (iTLC) scanning profile and ^{177}Lu-chelating stability.

accumulation. This can be achieved by avoiding rapid excretion via the renal route.[8] Dosing with long-circulating nanoparticles will distribute the off-target radiation as a whole-body dose, instead of accumulating it in eliminating organs. For instance, the minimal kidney excretion circumvents radiation-induced kidney toxicity, an issue in many existing radionuclide therapies.

RESULTS AND DISCUSSION

Synthesis, Characterization, and Labeling of SN201. The chemistry of the core formation is a condensation polymerization of a bis-phosphonate bissilane precursor monomer in aqueous ethylene glycol. The particle size can be controlled well in the synthesis simply by the starting concentration of the monomer, and the dispersity is acceptable for a pharmaceutical product. A thin layer of a second bissilane is then applied to improve the aqueous stability of the coated product. The coating consists of di-polyethylene glycol (PEG)-di silane (Figure 1A), which allows for a dense coating and superior long-term stability. The material is described in detail in the patent applications (EPO22160866.4, EPO22160879.7, EPO22160889.6, and EPO22160908.4), but a short discussion will be given below.

The chelating properties of the core allow for a practical labeling procedure. However, the polymeric nature of the chelator offers several chelating sites for Lu^{3+} of different affinities. This is because the phosphonate groups are oriented randomly to form chelating sites with slightly different geometries. To optimize the radiolabeling, we developed a two-step procedure of ^{175}Lu-SN201 (non-radioactive) and ^{177}Lu-SN201 (radioactive) materials. First, the Lu isotope is introduced to the nanoparticles at acidic pH, where the

phosphonate groups in the core are protonated. The acidic conditions reduce the affinity of Lu^{3+} to the nanoparticles but allow rapid binding kinetics. In the second step, the pH is brought up to neutral, and the Lu^{3+} ions get locked into the high-affinity sites, which have a low off-rate.

Stable radiochemical purity and chelating strength are two critical parameters of radiolabeled products. The as-made SN201 has a volume-weighted average size of 27 nm in diameter (Figure 1B). Moreover, the size stays similar after chelating to trivalent metal ions such as ^{177}Lu^{3+}. In order to assess the size distribution of the as-made SN201, size exclusion chromatography (SEC) combined with various biological and polymer standards was used. Relative to the standards, it can be concluded that 6.6% of SN201 has a size between PEO165 kDa and PEO1000 kDa. Furthermore, 90.5% of SN201 is between thyroglobulin and PEO165 kDa, and 2.9% of SN201 is between thyroglobulin and bovine serum albumin (BSA). The retention time of SN201 corresponds to that of *cowpea mosaic* virus-like particles (CPPV) with hydrodynamic diameters of 28−30 nm (Figure 1C).

To investigate the radio stability of the labeled nanoparticles, ^{177}Lu-SN201, with an activity of approximately 250 MBq/mL, was stored at ambient temperature for 5 days and analyzed by instant thin layer chromatography (iTLC) (Figure 1D). iTLC shows that more than 99% of ^{177}Lu is bound to SN201 and remains so over 5 days. The radiochemical purity and chelating strength of ^{177}Lu-SN201 fulfill the requirements of a clinical product. Furthermore, the chelating stability, assessed by a competitive binding test with diethylenetriaminepentaacetic acid (DTPA), remains similar after 5 days of storing the radiolabeled product. Pharmacokinetics of ^{177}Lu-SN201 aged up to 7 days post-labeling were not significantly different from
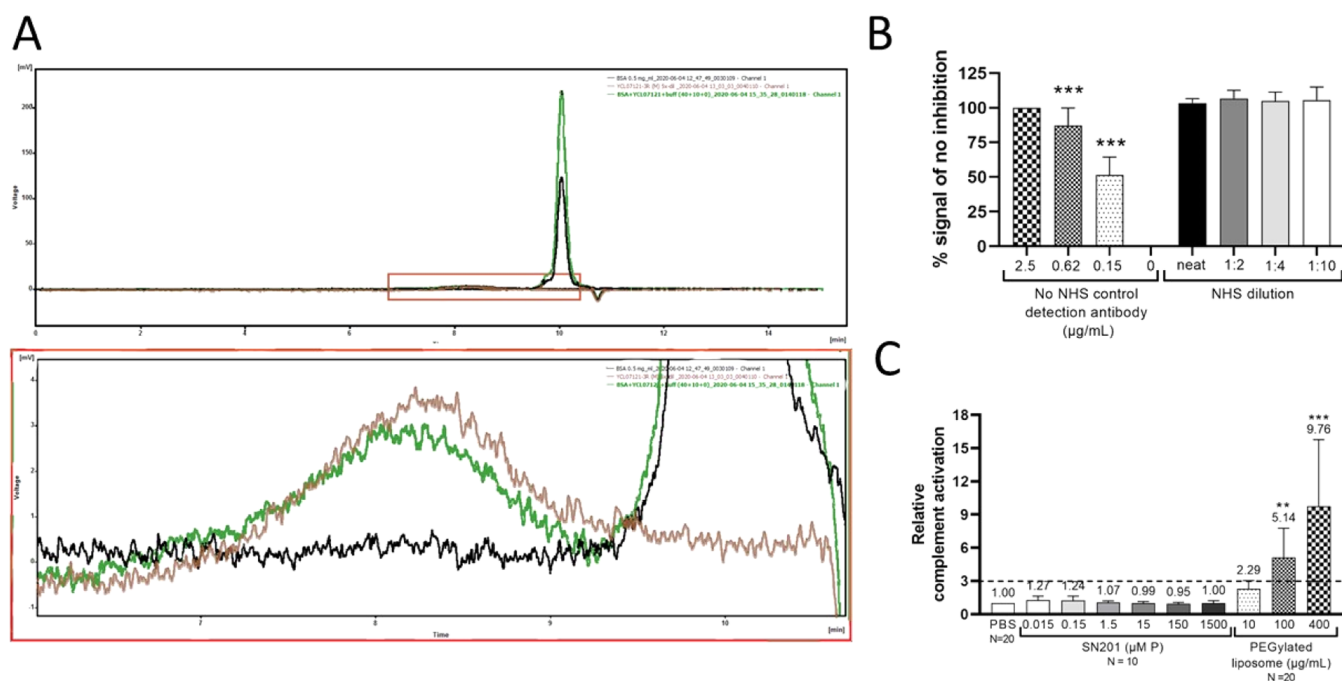
Figure 2. In vitro stealth properties of SN201. (A) 220 nm SEC-UV nanoparticle SN201 (brown), 8 μM BSA (black), and a mixture of 12 μM BSA with 0.08 μM SN201 (green). (B) Inhibition ELISA in which NHS was used to prevent the binding between SN201 and the detection antibody. (C) Relative complement activation in human serum ($n = 20$) after 1 h incubation with SN201. The dashed line denotes the clinically relevant complement activation. **, **, ** = $P < 0.01$; ***, ***, *** = $P < 0.001$.
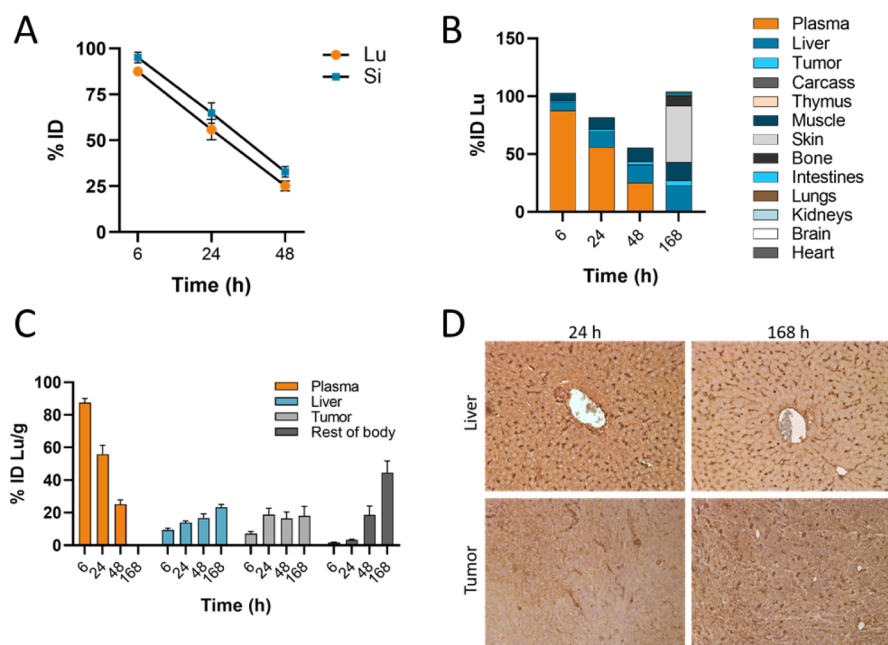

Figure 3. EPR mechanism of action of SN201. (A) Plasma % ID Lu and Si, (B) Lu % ID mass balance, and (C) tissue % ID Lu biodistribution at 6, 24, and 48 h after intravenous administration of [175]Lu-SN201 (2 μmol Lu/kg) to 4T1 tumor-bearing BALB/c female mice ($n = 5$). The "rest of the body" compartment represents the % ID Lu sum in the remaining organs that were sampled. (D) Representative IHC images presenting [175]Lu-SN201 distribution in the liver and tumor 24 and 168 h after intravenous administration.

those of freshly labeled nanoparticles (Figure S1). The radio stability profile aligns with the demands for a radioisotope pharmaceutical product.

In Vitro Stealth Properties of SN201. PEG is a synthetic polymer widely used to increase medicinal products' circulation time and biocompatibility. We designed SN201 to minimize interactions with cell membranes and plasma components. These requirements were fulfilled by grafting a layer of PEG onto the surface of the nanoparticles with a density of 1 PEG (2 kDa)-chain per nm². This is in line with the PEG density of other long-circulating PEGylated nanoparticles.[9] Even though free PEG is weakly immunogenic, some PEGylated pharmaceuticals exhibit strong immunoge-

nicity. For instance, PEG−protein conjugates induced anti-PEG antibody production in humans.[10]

The stealth properties of SN201 were evaluated in vitro before in vivo testing.[11] Unspecific protein binding to SN201, which could inhibit efficacy, was examined by SEC after incubation with BSA. The signal for BSA adsorbed onto SN201 was below the limit of detection of the chromatography instrument (Figure 2A). An inhibition enzyme-linked immunosorbent assay (ELISA) further investigated the interaction between serum proteins and SN201. SN201 was incubated with normal human serum (NHS) before detection by the anti-PEG antibody. The serum did not reduce the ELISA signal compared to the control [phosphate buffered saline (PBS)] (Figure 2B). The strong ELISA signal in the presence of serum suggests that interactions between SN201 and human serum components are weak or nonexistent.

Complement activation is a known issue for PEGylated nanomedicines. For example, Doxil, a chemotherapy medication with a PEGylated liposome vehicle, is known to activate the complement system.[11] SN201 was subjected to a complement activation assay, with Doxil as a positive control. SN201 did not significantly induce a clinically relevant activation of the complement system (Figure 2C). Moreover, SN201 was neither distributed into human red blood cells, nor did it cause hemolysis in vitro. The particles were also not cytotoxic to RAW264.7 macrophage cells after 72 h incubation (Figure S2).

Overall, results from the SEC analysis, inhibition ELISA, and complement activation test suggest that SN201 does not interact with major serum proteins or the complement system. Therefore, SN201 is biocompatible and bioinert in human blood.

SN201 Mechanism of Action. As described earlier, SN201 is designed to rely on the accumulation of lesions displaying the EPR effect. The rationale of EPR-targeted nanomedical concepts relies on physiological transfer into lesions characterized by leaky vasculature and poor lymphatic drainage.[7] Macromolecules at a size of 1−100 nm[12] accumulate via the EPR effect into compartments with increased vascular permeation, such as solid tumors. Based on the prolonged circulation time[13] that PEGylation enables in combination with the EPR effect, we postulated that ^{175}Lu-SN201 would mainly distribute to the tumor.

The targeting mechanism of SN201 was confirmed in vivo by administering ^{175}Lu-labeled SN201 intravenously to BALB/c mice bearing 4T1 mammary tumors. Plasma samples were analyzed for Lu and Si by inductively coupled plasma optical emission spectroscopy (ICP−OES) elemental analysis. The pharmacokinetic profile of ^{175}Lu in blood revealed that the circulation half-life for ^{175}Lu-SN201 was 23 h (Lu) and 27 h (Si). Furthermore, the two elements decreased at a similar rate, suggesting no dissociation between SN201 and ^{175}Lu (Figure 3A). An extended circulation time is desirable for nanoparticles to accumulate in tumors via the EPR effect selectively. Plasma ^{175}Lu was completely cleared 7 days post-treatment, with elemental distribution into various organs and tissues (Figure 3B). The mass balance study shows only a minor material loss over time. One explanation is that the excreted nanoparticles in the feces and urine are not included in the mass balance. The organ concentrations were calculated using literature values for organ and terminal tumor weights. The concentration in tumors stabilized at approximately 20% ID/g after 24 h (Figure

3C). The tumor uptake motivated the initiation of in vivo efficacy studies.

In line with the tumor uptake of ^{175}Lu-SN201, positive anti-PEG staining confirmed nanoparticle uptake from 24 h up to 168 h post-treatment. Apart from the tumor uptake, homogeneous staining was observed throughout the liver (Figure 3D). It is known that nanoparticles with a size larger than 7 nm are predominantly excreted via the hepatobiliary route.[14] Kupffer cells are responsible for removing inert macromolecules in the liver.[15] We concluded that the intense positively stained cells in the liver are supposedly Kupffer cells, whereas diffuse staining is present in hepatocytes.

In summary, the biodistribution data shows that the intact nanoparticles are delivered to the target via the proposed mechanism of action, the EPR effect. Although the injected dose concentration is distributed from the plasma to other organs, the nanoparticles accumulate in the tumors over 24 h and are then retained for at least 168 h post-treatment.

Dose Range Finding and Anti-Tumor Efficacy of ^{177}Lu-SN201. To explore the efficacy of ^{177}Lu-SN201, we first conducted a dose range-finding study with the 4T1 tumor model. After treating the mice with 0, 2.5, 5, and 20 MBq ^{177}Lu-SN201, the median survival time was 10, 13, and 13 days after treatment, respectively. Mice administered with PBS served as a control with a median survival time of 13 days. Histological analysis of representative livers from mice in all treatment groups confirmed uptake in the tumor and liver, as expected (Figure S3). One aim of the dose-range setup was to assess toxicity from the selected doses. Assessment of clinical chemistry and blood hematology of mice on the day of termination indicated the clinical toxicity profile of ^{177}Lu-SN201 doses. Not unexpected after radiation,[16] the white blood cell count was significantly reduced in all treatment groups compared to that in the control (20 MBq, 0.17 K/μL; 5 MBq, 9.9 K/μL; 2.5 MBq, 9.2 K/μL versus 0 MBq, 117 K/μL, $p < 0.05$ for all). Mice treated with 20 MBq had significantly elevated levels of total bilirubin compared to PBS-treated mice (20 MBq, 2.5 μmol/L; vehicle, 0.6 μmol/L, $p = 0.04$) and depleted platelets and red blood cells, denoting radiation-induced liver damage.[17] Treatment with 5 MBq resulted in a reduced platelet count, but red blood cells remained unchanged, compared to 0 MBq treatment. None of the chosen doses justified further testing; 20 and 5 MBq showed signs of radiation-induced toxicity, and 2.5 MBq did not show anti-tumor efficacy. To avoid toxicity and still achieve anti-tumor efficacy, we reasoned that a dose slightly less than 5 MBq but higher than 2.5 MBq/mouse would inhibit tumor growth without radiation-induced toxicity.

An evident problem with the 4T1 tumor model was severe skin ulcerations leading to the loss of several animals in all groups. It was observed in a study that skin ulcerations developed in ∼70% of mice with 4T1 tumors, regardless of tumor volume.[18] Noteworthily, it has been established that BALB/c mice are radiosensitive due to an unknown autosomal recessive genetic locus.[19] To overcome the skin ulceration issues and reduce the risk of radiotoxicity, we proceeded with the syngeneic MC38 adenocarcinoma tumor model in another wild-type mouse strain, C57BL/6 mice.

In the following study, the main focus was on anti-tumor efficacy and survival. Tumor volumes, body weight, vital signs, terminal clinical chemistry, hematology, and histology were recorded in MC38 tumor-bearing mice receiving ^{177}Lu-SN201 with an activity of 4 MBq or non-radioactive SN201. The
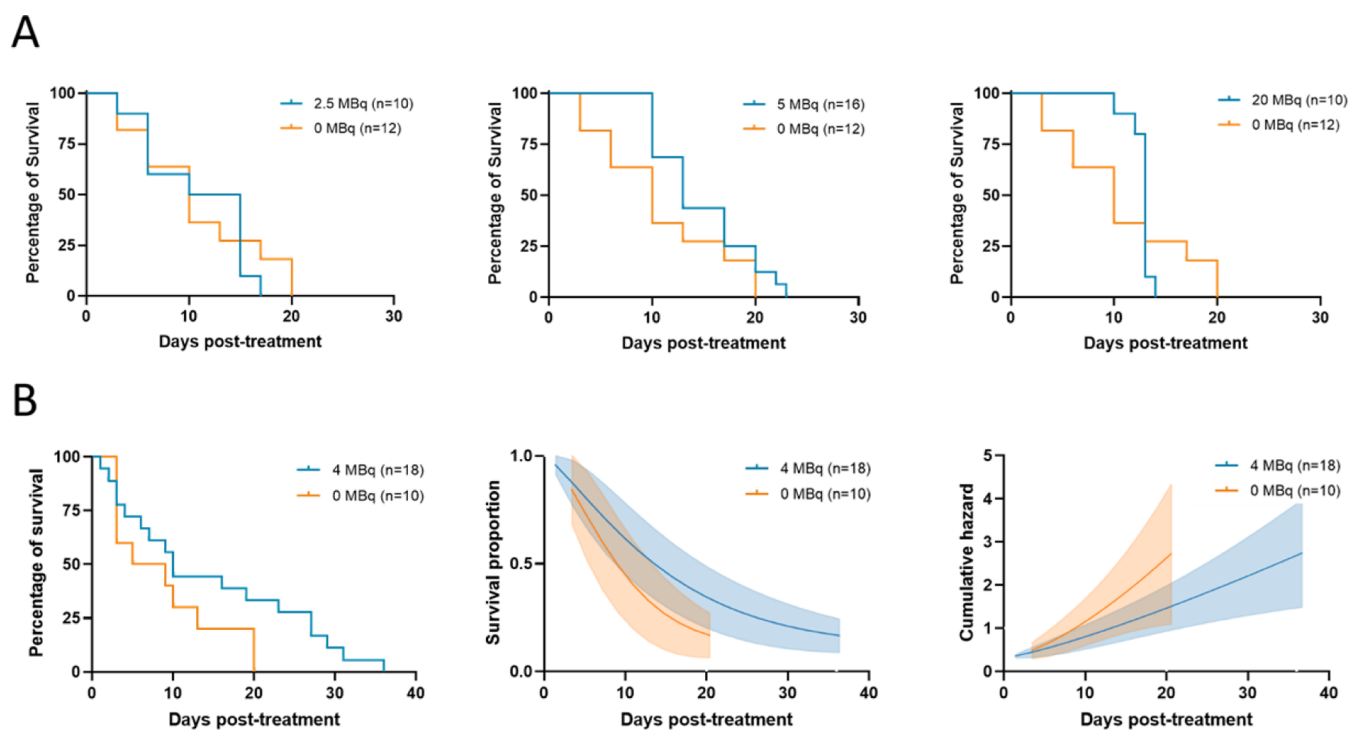
Figure 4. In vivo dose range finding and survival in tumor-bearing mice. (A) Survival after treatment with 2.5 (n = 10), 5 (n = 16), and 20 (n = 10) MBq/mouse ^{177}Lu-SN201, compared to that in the 0 MBq vehicle (n = 12) in 4T1 tumor-bearing mice. (B) Survival after treatment with ^{177}Lu-SN201 at 4 MBq (n = 18) or the vehicle (n = 10). The survival is presented as the uncensored graph (left), Weibull-fitted survival proportion (center), and cumulative hazard (right) over time.
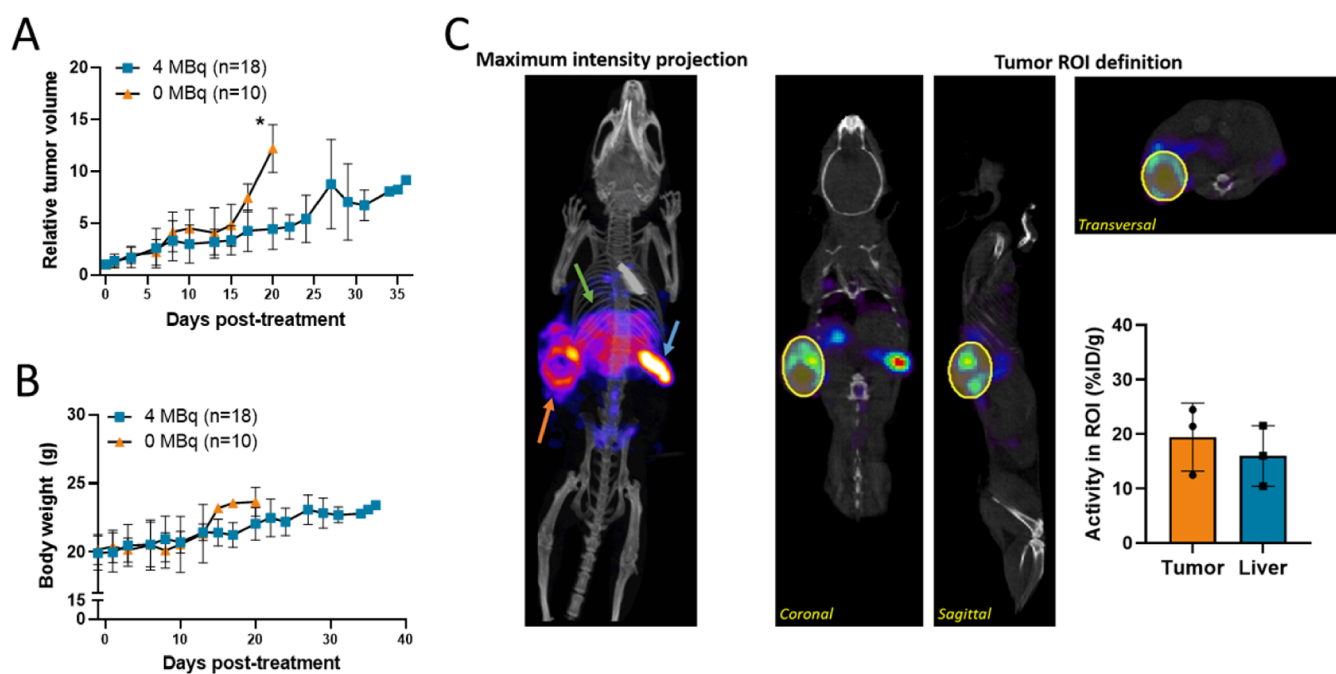

Figure 5. Anti-tumor efficacy and SPECT/CT imaging of ^{177}Lu-SN201. (A) Mean body weight ± SD and (B) relative tumor volume in MC38 tumor-bearing mice after treatment with 4 MBq/mouse (n = 18) ^{177}Lu-SN201 vs vehicle (n = 10). (C) Representative SPECT/CT images of maximum intensity projection and tumor region of interest (ROI) definitions in the coronal, sagittal, and transverse view, 72 h post-treatment with 4 MBq ^{177}Lu-SN201 in MC38 tumor-bearing mouse. The graph presents % ID/g in the ROIs, where bars show the mean ± SD error from n = 3 representative animals per timepoint. Arrows; orange, tumor; green, liver; and blue, spleen.

median survival was 10 days after treatment, whereas the vehicle had a mean survival of 7 days (Figure 4B, left). A Weibull parametric distribution was fitted to the survival data to estimate the survival proportions (Figure 4B, center) and

cumulative hazard (Figure 4B, right). Regression analysis provided a survival proportion coefficient of 15.58 days for the ^{177}Lu-SN201-treated group and 9.87 for the SN201 vehicle group. Thus, the ^{177}Lu-SN201 treatment prolongs the median

survival time by 37%, relative to the control. Translated to an equivalent human life span where 8.82 days equal 1 mouse year, the treatment will theoretically prolong a human's life by 5 months.[20]

Mice treated with ^{177}Lu-SN201 showed a reduced tumor growth rate without signs of radiotoxicity. The best-fit values of tumor doubling time are 11 days for the ^{177}Lu-SN201-treated and 6 days for the vehicle-treated group ($p < 0.05$) (Figure 5A). In addition, the body weight of the mice increased over time in the vehicle group but not in the ^{177}Lu-SN201 group (Figure 5B). However, when the body weights were adjusted to exclude the weight of the tumors, no statistical difference was shown between the treatment groups (Figure S4).

Three animals per timepoint were imaged in the SPECT/CT system to evaluate organ uptake and concentrations of ^{177}Lu-SN201 3 days post-treatment. The SPECT images showed relative activity concentrations in the tumor tissue of 12.5, 21.4, and 24.4% ID/g. In addition, the liver uptake was 10.4, 16.0, and 21.5% ID/g (Figure 5C). The SPECT quantification of tumor uptake is in line with the elemental analysis of ^{175}Lu-SN201 (16.4% at 48 h, 18.1% at 168 h, Figure 3C). In comparison, the maximum tumor uptake of ^{177}Lu-DOTATATE was 17.6% ID/g in mice with xenografts. Interestingly, clinical evidence of ^{177}Lu-DOTATATE given to patients with midgut neuroendocrine tumors had an interim survival rate of 65.2% at the 20 month cut-off date,[21] which encourages proceeding into clinical trials with ^{177}Lu-SN201. However, the biodistribution and effects of ^{177}Lu-SN201 and ^{177}Lu-DOTATATE cannot be directly compared due to their different targeting mechanisms. Although activity accumulation of ^{177}Lu-SN201 in the spleen is high, it is usually not considered an organ of concern in radiotherapy.[22]

CONCLUSIONS

This work is a proof-of-concept study demonstrating that ^{177}Lu-SN201 effectively targets and treats solid tumors via the EPR effect. A dose of 4 MBq per mouse resulted in anti-tumor efficacy, prolonged survival, acceptable toxicity, and clinically relevant SPECT imaging, indicating that ^{177}Lu-SN201 could be used as a theranostic. The material is biocompatible with no detectable protein binding and displays good radio- and serum stability. In addition, the long circulation half-life of SN201 allows for physiological tumor targeting.

In summary, we have shown that ^{177}Lu-SN201 is a new promising candidate drug for physiologically targeted radiotherapy of solid tumors.

EXPERIMENTAL SECTION

Synthesis of SN201. The synthesis of SN201 is carried out in three stages: synthesis of the nanoparticle core, priming of the core particles, and coating of the primed particles. The core nanoparticle is formed through a hydrolytic condensation polymerization of 1,7-bis(triethoxysilyl)-4,4-bis(dimethyl phosphonato)heptane (Figure S5), in aqueous ethylene glycol at elevated temperature. The core nanoparticle is primed with bis(triethoxysilyl)methane (BTESM), prior to coating. Coating of the primed nanoparticles is achieved through a slow addition of a solution of 1,7-bis(triethoxysilyl)-4,4-bis[ω-methyl-(ethyleneoxy)$_{45}$-methyl]-heptane, **SI-5**, to a diluted solution of the primed nanoparticles. The nanoparticle solution is filtered through a series of filters of decreasing pore size prior

to solvent exchange through tangential flow filtration (TFF), to yield SN201 as an aqueous solution free of organic solvents.

SI-5 is synthesized in two steps from 2,2-diallyl-propane-1,3-diol, **SI-2**, and mPEG-tosylate with an average molecular weight of 2000, **SI-3**.

Synthesis of the Core Nanoparticle. A 5 L jacketed reactor was equipped with a mechanical stirrer, a temperature probe, and a reflux condenser topped with a connection to a vacuum-nitrogen manifold. The reactor was charged with 93.60 g of **SI-1** of a purity of 94.5% and 4501 g of 90.0% (v/v) aqueous ethylene glycol, prepared by mixing 4414.0 g of ethylene glycol with 440.5 g of ultrapure water. The solution was degassed. The mantle temperature was increased to 155 °C over a period of 30 min with stirring, during which the solution became clear. After 1.5 h at the set mantle temperature, a gentle reflux was obtained, and the mantle temperature was adjusted to 151 °C. The reaction mixture was kept at reflux for 47 h before being cooled down to 20 °C. The nanostructure solution was filtered through double glass fiber filters (GF/A).

Average diameter (DLS): 17.6 nm, [P](ICP−OES) = 69 mM, and [Si](ICP−OES) = 72 mM.

Priming of the Core Nanoparticles. A 5 L jacketed reactor equipped with a mechanical stirrer, a temperature probe, and a connection to a N$_2$/vacuum manifold was charged with 4338 g of the solution of core nanostructures. The mantle temperature was set to 100 °C, and when the inner temperature was above 99 °C, 116.48 g of BTESM was added. The mixture was stirred at 300 rpm for 5 min, after which the mixture was homogeneous, and the stirring speed was lowered to 150 rpm. Heating was continued for 4 h before the solution was cooled to ambient temperature and filtered through double glass fiber filters.

Average diameter (DLS) = 19.7 nm, [P](ICP−OES) = 64 mM, and [Si](ICP−OES) = 225 mM.

Coating of the Primed Nanostructures. A 10 L jacketed reactor equipped with a mechanical stirrer, a temperature probe, an addition funnel heated to 40 °C using a heating fan, and a reflux condenser topped with a connection to a N$_2$/vacuum manifold was charged with 6330 g of 90% aqueous ethylene glycol and 3902 g of the solution of primed nanostructures. The jacket temperature was set to 125 °C for 1 h before being lowered to 110 °C. A coating solution was prepared by dissolving 548.2 g of **SI-5** (prepared as described below) in 548.2 g of anhydrous ethanol under heating to 40 °C. When the inner temperature in the reactor reached 105 °C, 250 mL of the coating solution was added. The remainder of the coating solution was added slowly via the addition funnel at 50 mL/h. The jacket temperature was kept at 110 °C for 48 h after the initial addition of coating solution to the reactor before being cooled down to ambient temperature.

Filtration of the Coated Nanoparticles. The crude reaction mixture was transferred to a 20 L Nalgene jug. The reactor was rinsed with ultrapure water (5 + 4 L), and the washings were added to the reaction mixture. The solution was filtered through a filtration setup consisting of 1.2, 0.45, and 0.2 μm filter capsules connected in series, and the filters were washed with 3 L of ultrapure water. The filtered solution was purified by ultrafiltration using a 5400 cm^2 300 kD TFF filter until the concentration of ethylene glycol was below 500 ppm and then concentrated to 1.3 L.

Average diameter (DLS) = 27.4 nm, Đ$_d$ = 1.17, [P](ICP−OES) = 168 mM, and [Si](ICP−OES) = 665 mM.

Formulation of Filtered Coated Nanostructures. A mixture of 423 g of the solution of coated nanostructures, 1.24 g of thioglycerol, 369 mg of gentisic acid, and 35.0 g of glycerol was diluted to 1154 mL with ultrapure water. The solution was filtered through a 0.2 μm polyethersulfone filter. The solution was portioned into 5 mL vials, frozen, and stored at −70 °C.

Synthesis of SI-4, 4,4-Bis[ω-methyl-(ethyleneoxy)$_{45}$-methyl]-hepta-1,6-diene. **SI-2** (22 g, 0.1411 mol) was dissolved in anhydrous toluene (2.61 L) and cooled in an ice bath. When the inner temperature reached below 10 °C, NaH (23.7 g, 0.593 mol, 60% in mineral oil, 4.2 equiv) was added in three portions while maintaining the temperature below 10 °C. The slurry was then stirred at room temperature for 60 min and then added to an azeotropically dried solution of **SI-3** (1.071 kg, 0.9877 mmol, 3.5 equiv) in anhydrous toluene (2.61 L) under N$_2$ at 0 °C. The reaction mixture was heated to reflux overnight under N$_2$. The reaction was monitored by high-performance liquid chromatography (HPLC), and upon completion, the temperature was lowered to 15 °C, and the reaction was quenched by a dropwise addition of H$_2$O (70 mL). The pH of the crude reaction mixture was adjusted to between 5 and 7 with 1.0 M HCl (100 mL). The crude reaction mixture was split in two equal portions for practical reasons, and the two portions were extracted separately. Each half of the crude mixture was diluted with H$_2$O (7.14 L). The temperature was increased to 60 °C, and NaCl (540 g) was added. The mixture was then stirred for 45 min and extracted three times with EtOAc (2.1 L). To the remaining aqueous phase, NaCl (200 g) was added, and the mixture was again extracted three times with EtOAc (2.1 L). The last three extracted fractions had an acceptable product purity (HPLC) and were dried over MgSO$_4$ and filtered through double GF/A filters, and the was solvent evaporated. The resulting residues were pooled and dissolved in H$_2$O (2.0 L), and the pH was adjusted to pH 8 with an 0.8 M aqueous solution of NaHCO$_3$ (100 mL). The aqueous phase was extracted three times with dichloromethane (500 mL). The organic phases were dried over MgSO$_4$, filtered, and evaporated to obtain a white residue. Consequently, the extraction process was repeated for the other half of the crude mixture, and the final products of both extractions were pooled.

The extracted products from two similarly sized reactions were pooled to obtain **SI-4** [758 g, 66.36% yield, 96.8% purity (HPLC−ELSD)].

^{1}H-NMR spectrum (400 MHz, CDCl$_3$): δ 5.80 (m, 2H), 5.03 (m, 4H), 3.81 (m, 4H), 3.70−3.60 (s, 540H), 3.37 (s, 6H), 3.22 (s, 4H), 2.04 (d, 4H) (Figure S6).

Synthesis of SI-5, 1,7-Bis(triethoxysilyl)-4,4-bis[ω-methyl-(ethyleneoxy)$_{45}$-methyl]-heptane. To an azeotropically dried solution of compound **SI-4** in CDCl$_3$ (714 g, 0.172 mol) in toluene (5.5 L), freshly distilled triethoxysilane (1117 g, 6.88 mol, 40 equiv) was added at 22 °C under nitrogen. Karstedt's catalyst (25.34 mL, 2% in xylenes, 1.14 mmol, 0.0066 equiv) was added in 1 mL portions using a syringe over 30 min which resulted in an exotherm of ≤2 °C. The reaction mixture was left stirring at 22 °C under nitrogen overnight.

The reaction was monitored by ^{1}H-NMR for the disappearance of the olefinic protons (Figure S5). The solvent was then evaporated, and excess silane was removed by co-evaporating with anhydrous toluene (4 × 2.5 L). The residue was then redissolved in toluene (4.2 L), degassed with three cycles of vacuum/nitrogen, and stirred with activated SIR-200 resin (175 g) for 3 days at 60 °C to scavenge platinum. The

solution was filtered from the resin, and the resin was washed with toluene (3 × 2.8 L); the collected fractions were filtered through double GF/A filters and pooled, and the solvent was evaporated to obtain compound **10** as a white solid in quantitative yield [783.2 g, ≥99%, 94.4% purity (HPLC−ELSD)].

^{1}H NMR (400 MHz, C$_6$D$_6$): δ 3.88 (q, 12H), 3.70−3.40 (s, 400H), 3.14 (s, 6H), 1.68 (m, 4H), 1.59 (m, 4H), 1.23 (t, 18H), 0.79 (t, 4H).

DLS Analysis. Particle size distribution using DLS and zeta potential analysis was performed on Nano-Zetasizer (Malvern Instruments Ltd. with Zetasizer Software V7.04). The results were given as the average volume size, dV, (nm), as the average of seven sub-measurements.

SEC for SN201 and ^{175}Lu-SN201. Non-radioactive SN201 was analyzed using a YL9100 HPLC instrument with a UV detector and an ELSD (Alltech 3300) connected in series, after elution from an SEC column (Agilent Bio SEC 5, 1000 Å). An isocratic method with a running time of 15 min was used, and the mobile phase was 90% 50 mM ammonium acetate and 10% HPLC-grade acetonitrile. Human thyroglobulin (Sigma-Aldrich, no 9010-34-8), BSA (Sigma-Aldrich, no 633-03-4), and CPMV-like particles (Leaf Expression Systems, no LES-P0001) were used as reference standards to determine the size distribution of SN201 in fractions. The particle peak was divided into sections by the selected standards, and fraction percentages were obtained by the area percentage of the respective section.

SEC for ^{177}Lu-SN201. The ^{177}Lu-SN201 particle size was analyzed using 1260 Agilent HPLC with a UV and a radioactivity detector after elution from Agilent Bio SEC 5 1000 Å, SEC column. An isocratic method was used with 90% 50 mM ammonium acetate and 10% HPLC-grade acetonitrile. The samples were eluted for 15 min with the variable UV detector set to 254 nm and the LabLogic FlowRam PMT detector set to a high voltage of 800 V.

$^{175/177}$Lu Labeling of SN201. SN201 has a naturally chelating core that works as a strong chelator. A mixture of SN201 and $^{175/177}$LuCl$_3$ was kept at 60 °C for 1 h and then pH-adjusted with 2 M tris at pH 8. Then, the mixture solution was kept at 60 °C for another 2 h before being cooled down to ambient temperature. The mixture was then filtered through a 0.2 μm syringe filter. The as-made ^{177}Lu-SN201 was stored at ambient temperature at an activity concentration of approximately 250 MBq/mL and sampled for iTLC at different time points for stability assessment. The radiolabeling of ^{177}Lu to SN201 was carried out at Lund University Imaging Center (LBIC, Lund, Sweden) for characterization experiments and at Minerva Imaging AS (Ølslykke, Denmark) for in vivo experiments.

Instant Thin Layer Chromatography. After radiolabeling, ^{177}Lu-SN201 was dropped on the ITLC-SG strip (Agilent Technologies, Art# SGI0001) and analyzed with a LabLogic ScanRam TLC scanner using a photomultiplier tube (PMT) detector. Detector settings were as follows: lower limit 450 V, upper limit 4095 V, and high voltage 800 V. The iTLC method was defined as a 12 cm scan at 1 mm/s. The application line was pre-set to 1.3 cm and the solvent front line to 11.3 cm, corresponding to the length of the strip. To analyze the resulting chromatogram, the application line, 0−30 mm, was set as one region representing ^{177}Lu-SN201, and the solvent front line, 90−120 mm, was set to another region to

represent free ^{177}Lu. A region was integrated between 50 and 80 mm to find a baseline value of 3 cm.

Inhibition ELISA. A MaxiSorp (Thermo Scientific) plate was coated with either ^{175}Lu-SN201 or PBS overnight at RT. The next day, wells were washed with PBS, followed by blocking with 1% BSA in PBS for 1 h at RT. After blocking, wells were added to the NHS (N = 5) pooled. Next, the plate was incubated for 1 h before washing with PBS with 0.05% Tween-20. Afterward, SN201 was detected by rabbit α PEG B-47 (Abcam) and goat α rabbit-HRP (Novus). The assay was then developed using a one-step 3,3′,5,5′-tetramethylbenzidine substrate (Thermo Scientific), prior to measurement of absorbance at 450 nm using a plate reader (SpectraMax i3x, Molecular Devices).

In Vitro Complement Activation Assay. Normal human blood samples from 20 anonymous individuals (10 males and 10 females) were purchased from BioIVT (United Kingdom). Serum samples from each individual (BioIVT) were incubated with PBS (background), ^{175}Lu-SN201, or PEGylated liposomes for 1 h at 37 °C. After incubation, complement activation was terminated by adding 10 mM ethylenediaminetetraacetic acid (EDTA). The complement activation in samples was quantified by measuring the terminal complement complex (TCC) concentration using a TCC detection kit (SVAR).

Cell Lines and Animals. Female BALB/c AnNrj and C57BL/6Jrj (Janvier, France) mice were purchased at ages of 7−8 weeks and acclimatized for at least 1 week. The murine cancer cell lines 4T1 and MC38 were cultured in Roswell Park Memorial Institute-1640 + GlutaMAX, supplemented with 10% fetal bovine serum and 1% penicillin−streptomycin at 37 °C in a humidified incubator containing 5% CO_2. Each cell culture was harvested and suspended in Dulbecco's phosphate-buffered saline (DPBS) (confluency approximately 60−80%) for the inoculation. Before each inoculation, the cells were harvested (60−80% confluent), resuspended in DPBS, and kept on ice. Then, mice were anesthetized with isoflurane, 2−4% in 98% O_2, and inoculated for each experiment. After this, all mice were returned to their cages and monitored until they fully recovered from the anesthesia. All cell and animal experiments were performed at the contract research organization Minerva Imaging (Ölslykke, Denmark), according to their standard operating procedures and ethical permissions.

Pharmacokinetics and Biodistribution Study with ^{175}Lu-Labeled SN201 Nanoparticles in 4T1 Tumor-Bearing Mice. The 4T1 cells (100 μL, 0.5 × 10^6) were subcutaneously inoculated with a 27 G needle into the right flank above the hindlimb of 7−8 week old BALB/c AnNrj female mice (n = 19). Bodyweight and tumor size were measured with a caliper from day 5 after inoculation. If skin ulcerations on the tumor site appeared, the wound diameter was measured, and a description of the wound was noted. The tumor volume was estimated using the following formula: 0.52 (length × width^2), assuming that the tumor was shaped as an ellipsoid. When the average tumor size reached 200−300 mm^3, mice were randomized into treatment groups based on tumor size. The animals were weighed on the day of dosing and injected intravenously into the lateral tail vein with ^{175}Lu-SN201 (5 mL/kg). Mice were euthanized in groups of n = 5 at 6, 24, and 48 h and in a group of n = 4 at 168 h post-injection. Terminal blood was collected in pre-chilled lithium-heparin, stored on ice, and centrifuged at 5000g for 5 min before transferring the plasma to −80 °C in 1.5 mL Eppendorf tubes

until ICP−OES analysis. Tumors, organs, and tissues, including the remaining carcass, were extracted and weighed. For the preparation of histological specimens, half of the liver and the tumor were fixed in 4% formaldehyde for 48 h, followed by storage in 70% EtOH at 4 °C until further processing. For ICP−OES analysis, tissue and organs were placed in pre-labeled plastic zip lock bags and stored at −80 °C. Feces were placed in pre-labeled 1.5 mL Eppendorf tubes, frozen at −20 °C, and stored at −80 °C.

Dose-Range Titration of ^{177}Lu-Bound SN201 Nanoparticles in 4T1 Tumor-Bearing Mice. The 4T1 cells (100 μL, 0.5 × 106) were subcutaneously inoculated into the right flank above the hindlimb of 7−8 week old female BALB/c AnNrj mice (n = 40). The mice were randomized into treatment groups 14−15 days post-inoculation when the average tumor volume reached 200−300 mm^3. Animals were intravenously administered with ^{177}Lu-SN201 (2.5, 5, or 20 MBq/mouse). The injection dose volume was determined by measuring the syringe before and after injection with a dose calibrator (model, vendor, country). Survival of the mice was assessed, and mice were euthanized when they reached either humane end points in cases where the animals show signs of permanent suffering, pain, or fear or at the study end.

Efficacy of ^{177}LuSN201 (4 MBq) in MC38 Tumor-Bearing Mice. MC38 cells (100 μL, 0.5 × 10^6) were subcutaneously inoculated into the right flank above the hindlimb of 7−8 week old female C57BL/6Jrj mice (n = 40). The mice were randomized into treatment groups 17 days post-inoculation when the average tumor volume reached 100−150 mm^3. The tumor volume was calculated using the formula for calculating the volume of an ellipsoid 0.52(length × width^2) under the assumption of a tissue density of 1.0 g/cm^3. The width refers to the shorter of the two axes. The tumor growth inhibition was calculated as relative to the tumor volume at day 0 of treatment for each animal. Animals were intravenously administered with ^{177}Lu-SN201 (4 MBq/mouse). The injected dose in MBq was determined by measuring the syringe before and after injection with a dose calibrator (model, vendor, country). All visible signs of ill health and any behavioral changes were recorded. Mice were euthanized when they reached humane end points or at the study end. Terminal blood sampling was performed under anesthesia (sevoflurane, 2−4% in ambient air supplemented with 100% O_2 at an approximately 4:1 ratio) by cardiac puncture prior to cervical dislocation. Blood collected in EDTA tubes was analyzed on a hematology system on the sampling day. Hematology parameters were measured using a ProCyte Dx hematology analyzer (IDEXX) with mouse settings. Serum separator tubes were centrifuged at 2000 rpm for 10 min, and serum was transferred to prelabeled 1.5 mL Eppendorf tubes. Serum was left to decay in storage and was after decay shipped to an external laboratory for clinical chemistry analysis (University of Copenhagen, Department of Veterinary Clinical Sciences, Veterinary Diagnostic Laboratory). Clinical chemistry analysis of total bilirubin, creatinine, alkaline phosphatase, aspartate aminotransferase, alanine aminotransferase, and lactate dehydrogenase was performed on 250 μL of serum using an Advia 1800 Chemistry System (Siemens). For the histological tumor, liver, and lung preparation, the specimens were fixed in 4% formaldehyde for 48 h, followed by storage in 70% EtOH at 4 °C until further processing.

Immunohistochemistry Staining for Anti-PEG. All immunohistochemistry procedures were carried out by Micro-Morph (Lund, Sweden). The tissue samples were automatically dehydrated and embedded in paraffin in a TISSUE-TEK VIP (Miles Scientific) before being embedded in paraffin. Paraffin sections (4 μm) were prepared and dried in an oven at 37 °C overnight. The slides were subjected to deparaffinization and pretreatment antigen retrieval pH 9.0 (Dako, S2367) by boiling at 100 °C for 20 min and then cooling at RT for 20 min. The slides were then immersed in PBS for 5 min, following by blocking the sections with 5% normal goat serum. The rabbit anti-mouse PEG B-47 (Abcam, Ab51257) primary antibody was diluted 1:1000 in PBS + 5% normal goat serum for incubation of the sections with the antibody at RT for 1 h. Next, slides were washed 3× with PBS and incubated with the goat anti-rabbit HRP (immunologic, DPVR110HRP) secondary antibody for 30 min at RT. Then, slides were washed with Tris buffer 3×, and sections were incubated with 3,3′-diaminobenzidine for 5 min at RT, followed by hematoxylin counterstain, dehydration, and mounting of a cover slide.

SPECT/CT Imaging and Dosimetry. Six representative animals from the 4 MBq ^{177}Lu-SN201 group were subjected to SPECT imaging. The uptake and distribution of ^{177}Lu-SN201 were acquired with a dedicated small animal SPECT/CT system (nanoScan, Mediso, Hungary), a multi-pinhole, and a high-resolution system 3 and 10 days post-treatment. The animals were anesthetized with isoflurane and placed in the camera, and an 85 min SPECT measurement was performed. In conjunction with the SPECT measurement, a CT scan was also performed and used for fusion with the SPECT images for anatomical localization. After the acquisition, SPECT data were reconstructed using the Tera-Tomo 3D SPECT reconstruction engine (Nucline, Mediso, Hungary). Dosimetry of ^{177}Lu-SN201 in the tumor and liver was performed with Amide software. Coronal, transverse, and sagittal planes were defined manually for each region of interest (ROI) from the reconstructed image volume.

Statistics. Inhibition ELISA and in vitro complement activation assay were analyzed by one-way analysis of variance (ANOVA) and repeated measures ANOVA tests respectively. Clinical chemistry and hematology plasma markers measured from the animals on the day of termination were analyzed for equal variances between groups with one-way ANOVA and if significantly different, were followed by Student's one-tailed t-test assuming unequal variance. The tumor growth rates were analyzed by fitting the data to a least-squares exponential curve to find the doubling time. All statistical analysis was conducted using GraphPad Prism 9.0, except for the survival analysis. Survival was analyzed by fitting the data to Weibull distribution for median survival time. The cumulative hazard ratio was estimated using the maximum likelihood test statistics at a 95% significance level with the Python Lifelines module in Python 3.

ASSOCIATED CONTENT

Supporting Information

The Supporting Information is available free of charge at https://pubs.acs.org/doi/10.1021/acsomega.2c06755.

> Radio stability, hemato- and cyto-toxicity, immunohistochemistry, and tumor-compensated body weight 20 days post-treatment (PDF)

AUTHOR INFORMATION

Corresponding Author

Oskar Axelsson − *Spago Nanomedical, 223 63 Lund, Sweden;* orcid.org/0000-0003-3209-7241; Email: oskar.axelsson@spagonanomedical.se

Authors

Ingrid Yao Mattisson − *Spago Nanomedical, 223 63 Lund, Sweden;* orcid.org/0000-0002-5954-5334

Sania Bäckström − *Spago Nanomedical, 223 63 Lund, Sweden;* Present Address: NanoEcho AB, Gasverksgatan, 222 29 Lund, Sweden

Erik Ekengard − *Spago Nanomedical, 223 63 Lund, Sweden;* orcid.org/0000-0003-2052-762X

Sujinna Lekmeechai − *Spago Nanomedical, 223 63 Lund, Sweden*

Yi-Chi Liu − *Spago Nanomedical, 223 63 Lund, Sweden*

Juraj Paris − *Spago Nanomedical, 223 63 Lund, Sweden*

Rodrigo Petoral − *Spago Nanomedical, 223 63 Lund, Sweden*

Marie Sydoff − *Lund University Bioimaging Centre, 221 84 Lund, Sweden*

Mats Hansen − *Spago Nanomedical, 223 63 Lund, Sweden*

Complete contact information is available at:
https://pubs.acs.org/10.1021/acsomega.2c06755

Author Contributions

S.B., E.E., S.L., Y.-C.L., J.P., and R.P. contributed equally. Authors are sorted based on alphabetical order. O.A. and M.H. established the research question, hypotheses, and chemistry. Y.-C.L., O.A., J.P., and E.E. planned, executed, and analyzed the particle synthesis. In vitro characterization was planned and performed by S.L., Y.-C.L., O.A., and R.P. In vivo efficacy experiments were planned and outsourced by S.B., I.Y.M., and O.A. M.S., I.Y.M., and O.A. analyzed SPECT imaging data. The manuscript draft was written by I.Y.M., and the final manuscript was critically revised by S.L., Y.-C.L., M.S., and O.A. All authors have approved the final version of the manuscript.

Notes

The authors declare the following competing financial interest(s): IYM, SB, EE, SL, YCL, JP, RP, MH and OA are employed by Spago Nanomedical AB

ABBREVIATIONS

EPR, enhanced permeation and retention; SPECT, single photon emission computed tomography; MRI, magnetic resonance imaging; CPMV, *Cowpea mosaic* virus-like particles; BSA, bovine serum albumin; iTLC, instant thin layer chromatography; DTPA, diethylenetriaminepentaacetic acid; PEG, polyethylene glycol; SEC, size exclusion chromatography; ID/g, injected dose per gram

REFERENCES

(1) Wang, S.; Zeng, J.; Xiao, R.; Xu, G.; Liu, G.; Xiong, D.; Ye, Y.; Chen, B.; Wang, H.; Luo, Q.; Huang, Z. Poor Prognosis and SATB1

Overexpression in Solid Tumors: A Meta-Analysis. *Cancer Manage. Res.* **2018**, *10*, 1471−1478.

(2) Schirrmacher, V. From Chemotherapy to Biological Therapy: A Review of Novel Concepts to Reduce the Side Effects of Systemic Cancer Treatment (Review). *Int. J. Oncol.* **2019**, *54*, 407−419.

(3) Sgouros, G.; Bodei, L.; McDevitt, M. R.; Nedrow, J. R. Radiopharmaceutical Therapy in Cancer: Clinical Advances and Challenges. *Nat. Rev. Drug Discovery* **2020**, *19*, 589−608.

(4) Dash, A.; Knapp, F. F.; Pillai, M. Targeted Radionuclide Therapy - An Overview. *Curr. Radiopharm.* **2013**, *6*, 152−180.

(5) Kumar, C.; Shetake, N.; Desai, S.; Kumar, A.; Samuel, G.; Pandey, B. N. Relevance of Radiobiological Concepts in Radionuclide Therapy of Cancer. *Int. J. Radiat. Biol.* **2016**, *92*, 173−186.

(6) Jansen, G.; Gatenby, R.; Aktipis, C. A. Control vs. Eradication: Applying Infectious Disease Treatment Strategies to Cancer. *Proc. Natl. Acad. Sci.* **2015**, *112*, 937−938.

(7) Maeda, H. The 35th Anniversary of the Discovery of EPR Effect: A New Wave of Nanomedicines for Tumor-Targeted Drug Delivery—Personal Remarks and Future Prospects. *J. Pers. Med.* **2021**, *11*, 229.

(8) Mitchell, M. J.; Billingsley, M. M.; Haley, R. M.; Wechsler, M. E.; Peppas, N. A.; Langer, R. Engineering Precision Nanoparticles for Drug Delivery. *Nat. Rev. Drug Discovery* **2021**, *20*, 101−124.

(9) Adumeau, L.; Genevois, C.; Roudier, L.; Schatz, C.; Couillaud, F.; Mornet, S. Impact of Surface Grafting Density of PEG Macromolecules on Dually Fluorescent Silica Nanoparticles Used for the in Vivo Imaging of Subcutaneous Tumors. *Biochim. Biophys. Acta Gen. Subj.* **2017**, *1861*, 1587−1596.

(10) Mohamed, M.; Abu Lila, A. S.; Shimizu, T.; Alaaeldin, E.; Hussein, A.; Sarhan, H. A.; Szebeni, J.; Ishida, T. PEGylated Liposomes: Immunological Responses. *Sci. Technol. Adv. Mater.* **2019**, *20*, 710−724.

(11) Kozma, G. T.; Mészáros, T.; Weiszhár, Z.; Schneider, T.; Rosta, A.; Urbanics, R.; Rosivall, L.; Szebeni, J. Variable Association of Complement Activation by Rituximab and Paclitaxel in Cancer Patients in Vivo and in Their Screening Serum In Vitro with Clinical Manifestations of Hypersensitivity: A Pilot Study. *Eur. J. Nanomed.* **2015**, *7*, 289.

(12) Awasthi, K. K.; Awasthi, A.; Verma, R.; Soni, I.; Awasthi, K.; John, P. J. Silver Nanoparticles and Carbon Nanotubes Induced DNA Damage in Mice Evaluated by Single Cell Gel Electrophoresis. *Macromol. Symp.* **2015**, *357*, 210−217.

(13) Suk, J. S.; Xu, Q.; Kim, N.; Hanes, J.; Ensign, L. M. PEGylation as a Strategy for Improving Nanoparticle-Based Drug and Gene Delivery. *Adv. Drug Delivery Rev.* **2016**, *99*, 28−51.

(14) Zhang, Y.-N.; Poon, W.; Tavares, A. J.; McGilvray, I. D.; Chan, W. C. W. Nanoparticle−Liver Interactions: Cellular Uptake and Hepatobiliary Elimination. *J. Controlled Release* **2016**, *240*, 332−348.

(15) Sadauskas, E.; Wallin, H.; Stoltenberg, M.; Vogel, U.; Doering, P.; Larsen, A.; Danscher, G. Kupffer Cells Are Central in the Removal of Nanoparticles from the Organism. *Part. Fibre Toxicol.* **2007**, *4*, 10.

(16) Jameus, A.; Kennedy, A. E.; Thome, C. Hematological Changes Following Low Dose Radiation Therapy and Comparison to Current Standard of Care Cancer Treatments. *Dose-Response* **2021**, *19*, 155932582110561.

(17) Toesca, D. A. S.; Ibragimov, B.; Koong, A. J.; Xing, L.; Koong, A. C.; Chang, D. T. Strategies for Prediction and Mitigation of Radiation-Induced Liver Toxicity. *J. Radiat. Res.* **2018**, *59*, i40−i49.

(18) Pulaski, B. A.; Terman, D. S.; Khan, S.; Muller, E.; Ostrand-Rosenberg, S. Cooperativity of Staphylococcal Aureus Enterotoxin B Superantigen, Major Histocompatibility Complex Class II, and CD80 for Immunotherapy of Advanced Spontaneous Metastases in a Clinically Relevant Postoperative Mouse Breast Cancer Model. *Cancer Res.* **2000**, *60*, 2710−2715.

(19) Hanson, W. R.; Fry, R. J. M.; Sallese, A. R.; Frischer, H.; Ahmad, T.; Ainsworth, E. J. Comparison of Intestine and Bone Marrow Radiosensitivity of the BALB/c and the C57BL/6 Mouse Strains and Their B6CF 1 Offspring. *Radiat. Res.* **1987**, *110*, 340.

(20) Dutta, S.; Sengupta, P. Men and Mice: Relating Their Ages. *Life Sci.* **2016**, *152*, 244−248.

(21) Strosberg, J.; El-Haddad, G.; Wolin, E.; Hendifar, A.; Yao, J.; Chasen, B.; Mittra, E.; Kunz, P. L.; Kulke, M. H.; Jacene, H.; Bushnell, D.; O'Dorisio, T. M.; Baum, R. P.; Kulkarni, H. R.; Caplin, M.; Lebtahi, R.; Hobday, T.; Delpassand, E.; Van Cutsem, E.; Benson, A.; Srirajaskanthan, R.; Pavel, M.; Mora, J.; Berlin, J.; Grande, E.; Reed, N.; Seregni, E.; Öberg, K.; Lopera Sierra, M.; Santoro, P.; Thevenet, T.; Erion, J. L.; Ruszniewski, P.; Kwekkeboom, D.; Krenning, E. Phase 3 Trial of [177] Lu-Dotatate for Midgut Neuroendocrine Tumors. *N. Engl. J. Med.* **2017**, *376*, 125−135.

(22) Alexandru, M.; Rodica, A.; Dragos-Eugen, G.; Mihai-Teodor, G. Assessing the Spleen as an Organ at Risk in Radiation Therapy and Its Relationship With Radiation-Induced Lymphopenia: A Retrospective Study and Literature Review. *Adv. Radiat. Oncol.* **2021**, *6*, 100761.